PDE Modeling and Control of Electric Vehicle Fleets for Ancillary Services: A Discrete Charging Case

Caroline Le Floch, Emre Can Kara, Scott Moura

***Abstract*—This paper examines modeling and control of a large population of grid-connected plug-in electric vehicles (PEVs). PEV populations can be leveraged to provide valuable grid services when managed via model-based control. However, such grid services cannot sacrifice a PEV's primary purpose – mobility. We consider an aggregator, which can control a fleet of PEVs with three possible charging rates: charging at a constant rate, discharging at a constant rate or idle. We develop a system of coupled partial differential equations (PDEs) for aggregating large populations of PEVs and transform its discretized version into a state space representation. We propose a Linear Quadratic Regulator (LQR) to track a power signal that provides load following services. We investigate the sensitivity of controller parameters, different bidding strategies and their impact on the performance of the provided balancing service. We examine this control design on a simulated case study, and analyze sensitivity to a variety of assumptions and parameter selections.**

***Index Terms*—Aggregator, Linear Quadratic Control, Load Following, Partial Differential Equations, Vehicle-to-grid (V2G).**

I. Introduction

PEVs provide a compelling opportunity for supplying demand-side management services in the smart grid. Namely, a vehicle-to-grid (V2G) capable PEV communicates with the grid, stores energy, and can return energy to the electric grid. If properly managed, PEVs can enhance energy infrastructure resilience, enable renewable integration, and reduce economic costs for consumers and energy providers [1]. In addition to these societal-level infrastructure and environmental benefits, V2G strategies may provide additional revenue streams to PEV owners [2]. Underscoring this opportunity, U.S. personal vehicles are parked and un-used 96% of time [3]. A single PEV typically charges or discharges at 5-20 kW, which is insufficient to participate in power grid markets. However, populations of PEVs can be aggregated to collectively provide grid services [4]. The main challenge, however, is monitoring and managing a large population of distributed PEV resources without sacrificing their primary function of personal mobility. As such, this paper examines modeling and control of grid integrated PEV populations.

C. Le Floch and S. Moura are with the Energy, Controls, and Applications Laboratory (eCAL) in the Department of Civil and Environmental Engineering at the University of California, Berkeley, CA 94720, USA (e-mail: caroline.le_floch@berkeley.edu, smoura@berkeley.edu)

E. C. Kara is with the Grid Integration Group at the Energy Technologies Area, Lawrence Berkeley National Laboratory

This work was supported in part by the Siebel Energy Institute.

A growing body of literature addresses design of charging algorithms for PEV control, and base their method on different charging infrastructure scenarios: either a continuous or discrete charging rate. In the first case, the charging rate takes values in a continuous range and both centralized algorithms [5], [6] and distributed algorithms [7]–[10] have been proposed to compute optimal load profiles. Distributed optimization leads to protocols where each PEV solves a local problem and communicates independently to a central system. This distributed architecture is particularly adapted to large scale systems. However, in reality, the vast majority of electric vehicle supply equipment only enables a discrete range of charging rates. For example, the North American standard SAE J1772 defines two types of charging rates: AC Level 1 chargers provide charging through 120V AC plugs and AC Level 2 chargers provide charging through 240V or 208V AC plugs [11]. In practice, this leads to combinatorial optimization problems, where the aforementioned distributed methods are not applicable, and where direct centralized algorithms are intractable to study large systems. In this case, available methods include unit commitment [12], simulation-based algorithms [5], stochastic protocols [13] or dynamic programming [14]. However, for all these methods, the problem becomes harder to solve as the number of PEVs grows: either the convergence time increases or the optimality of the computed solution decreases.

In this paper we examine a significantly different approach for PEV charging with discrete charging rates that utilizes partial differential equations (PDEs). Rather than modeling each agent individually, we use aggregation methods to model and control the population dynamics [15], [16]. Continuum models have been largely applied to the case of Thermostatically Controlled Loads (TCLs) where PDEs represent the diffusion of air conditioning loads$'$ temperatures within the deadbands of their thermostats [17]–[19]. In this paper we use a similar modeling framework and consider a PEV as a load, which diffuses along the State Of Energy (SOE) axis. We utilize a discretized form of PDEs and propose a novel state space model, where we can control flows between different discrete charging rates. Contrary to other methods, the complexity of our problem does not depend on the number of agents, and the accuracy of the model increases as the number of PEVs increases. The main contributions of the article are the following:

- We propose a novel state-space modeling framework for

TABLE I. PDE aggregation symbols

Symbol	Description
x	PEV battery SOE
t	Time
$u(x,t)$	Density of charging PEVs (nb of PEVs per SOE)
$v(x,t)$	Density of idle PEVs (nb of PEVs per SOE)
$w(x,t)$	Density of discharging PEVs (nb of PEVs per SOE)
$\sigma_{i\to c}(x,t)$	Flow of PEVs from Idle to Charge
$\sigma_{i\to d}(x,t)$	Flow of PEVs from Idle to Discharge
$\sigma_{i\to Or}(x,t)$	Net Flow of PEVs from Idle to On Road

large fleets of PEVs, via aggregation and continuum modeling.

- We formulate a Linear Quadratic Regulator (LQR), and use Model Predictive Control (MPC) techniques to track a power reference signal with PEVs. To the best of our knowledge, power and voltage signal tracking with MPC methods has been proposed for continuous charging rate [20], [21] or semi continuous charging rate [22], but this is new to the field of PEV control with discrete charging rate.

The remainder of the paper is organized as follows. Section II develops a system of coupled PDEs to model PEV aggregations. Section II transforms the discretized version of this system into a state space model and proposes a model predictive controller to track a power signal. Section IV presents different case studies, shows how to tune the LQR parameters, and explores the problem of maximum capacity bidding.

II. Modeling Aggregations of PEVs

We seek to model a large homogeneous population of N discrete PEVs as a continuous representation, mathematically represented by three coupled PDEs. PEVs in the population fall into three discrete states:

- *Charging*: a PEV receives energy from the grid (Grid-to-Vehicle or G2V)
- *Idle*: a PEV is plugged-in but does not charge, nor discharge.
- *Discharging*: a PEV gives energy to the grid (Vehicle-to-Grid or V2G)

Each discrete state will be described by a transport PDE, i.e. a first order hyperbolic PDE. The aggregator controls how PEVs switch from one discrete state to another. This ultimately renders coupling terms and forms a system of three coupled transport PDEs.

A. PDE model

Consider a large homogeneous population of plugged-in PEVs over the State of Energy (SOE) interval $[0,1]$ at some fixed time, as visualized by Fig. 1. PEVs can be in three states: charge $u(x,t)$, idle $v(x,t)$, and discharge $w(x,t)$. The σ terms model PEVs moving between individual states $\sigma_{i\to c}, \sigma_{i\to d}$, and between states and the environment, i.e. checked-in or out by drivers on the road $\sigma_{i\to Or}$. The three states described above (i.e. charging, idle and discharging) only account for plugged-in PEVs. Hence, this framework does not model the dynamics

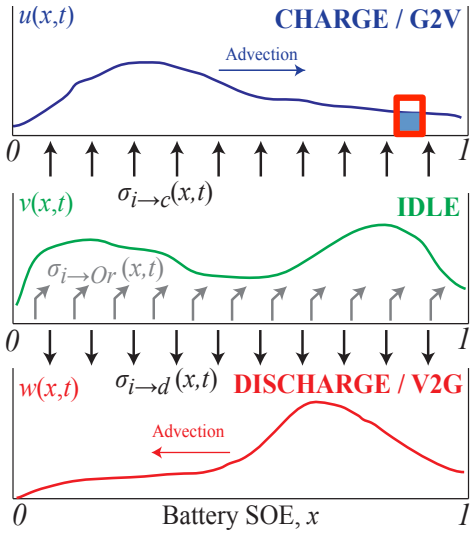

Fig. 1. PEV population state dynamics (see zoom on Fig. 2)

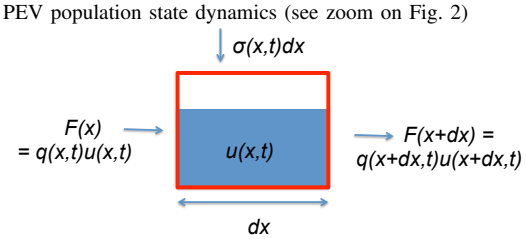

Fig. 2. Zoom over an infinitesimal segment of charging PEVs: flows between x and $x+dx$

of cars that are on the road (uncontrollable). Instead, the contribution coming from departures and arrivals is modeled by the uncontrollable flow $\sigma_{i\to Or}$.

To derive this aggregated PDE population model, we consider a simple PEV battery model. Denote the i'th PEV battery SOE and power by $x_i(t)$ and $P_i(t)$, respectively. Then a simple battery model is given by

$$\dot{x}_i(t) = \frac{\eta^m(x_i)}{E_{\max}} P_i(t), \qquad i = 1,\cdots,N, \tag{1}$$

$$m = \begin{cases} 1 & \text{if } P_i(t) \geq 0, \\ -1 & \text{if } P_i(t) < 0, \end{cases} \tag{2}$$

where $E_{\max}$, η, N are parameters that represent the battery energy capacity, power conversion efficiency, and PEV population size. Efficiency $\eta \in [0,1]$ is generally a function of SOE x_i. We assume $E_{\max}$ and η are homogeneous across the entire population. In this article we choose to express x in terms of SOE instead of SOC because dx/dt is linearly related to power.This provides a linear model (see Eq.1) that is amenable to the aggregation process we employ to derive a PDE. Note that unit-wise, dx/dt is normalized kWh. Furthermore, the cumulative power consumption from charging and power generation from discharging is given, respectively, by

$$P_c(t) = \sum_{i=1}^{N} P_i \cdot \mathbb{1}(P_i > 0), \quad P_d(t) = \sum_{i=1}^{N} P_i \cdot \mathbb{1}(P_i < 0), \tag{3}$$

where $\mathbb{1}(\cdot)$ is the indicator function. More complex battery models could be considered in future work.

Consider an infinitesimal segment of $u(x,t)$ as shown in Fig. 2. The number of charging PEVs at SOE level x at time t is denoted by $u(x,t)$ and charge at rate $q_c(x,t) = \eta(x)/E_{\max} \cdot P(t)$. We seek to model the evolution of the number of charging PEVs contained in the infinitesimal volume between x and $x+dx$. Let $F(x,t)$ denote the flow of PEVs at SOE x and time t, the entering flow and exiting flow are respectively:

$$F(x,t) = q_c(x,t)u(x,t), \quad (4)$$
$$F(x+dx,t) = q_c(x+dx,t)u(x+dx,t). \quad (5)$$

An additional flow of PEVs from the idle state to charging state are denoted $\sigma_{i\to c}(x,t)$ (see Fig. 1). As illustrated in Fig. 2, $u(x,t)dx$ is an approximate measure of the number of PEVs with SOE between x and x+dx at time t. Therefore, the conservation law during the infinitesimal time interval dt gives:

$$[u(x,t+dt) - u(x,t)]dx = \quad (6)$$
$$q_c(x,t)u(x,t)dt - q_c(x+dx,t)u(x+dx,t)dt + \sigma_{i\to c}(x,t)dt.$$

In Eq. 6, PEVs should pass through the idle state to go from the G2V state to the V2G state. When $dt \to 0$ and $dx \to 0$, the relation becomes:

$$\frac{\partial u}{\partial t}(x,t) = -\frac{\partial}{\partial x}[q_c(x,t)u(x,t)] + \sigma_{i\to c}(x,t). \quad (7)$$

PDEs for the idle and discharging are similarly derived as

$$\frac{\partial v}{\partial t}(x,t) = -\sigma_{i\to or}(x,t) - \sigma_{i\to c}(x,t) - \sigma_{i\to d}(x,t), \quad (8)$$
$$\frac{\partial w}{\partial t}(x,t) = \frac{\partial}{\partial x}[q_d(x,t)w(x,t)] + \sigma_{i\to d}(x,t). \quad (9)$$

B. Boundary Conditions

For the system to be well posed, we need to define boundary conditions at $x = 0$ for $u(x,t)$ and $x = 1$ for $w(x,t)$ [23]. We set the following Dirichlet conditions:

- $u(0,t) = 0$: no flow of charging PEVs from the SOE range $x \leq 0$.
- $w(1,t) = 0$: no flow of discharging PEVs from the SOE range $x \geq 1$.

In addition, we must define boundary values for $q_c(x,t)$ and $q_d(x,t)$ to ensure physical meaning of the system:

- $q_c(1,t) = 0$: no charging at $x = 1$.
- $q_d(0,t) = 0$: no discharging at $x = 0$.

Figure 3 illustrates the PDE dynamics with the above boundary conditions. It shows the uncontrolled evolution of the PEV fleet during four hours when the boundaries of the system are $SOE \in [0.5,1]$. In this case $\sigma_{i\to c} = \sigma_{i\to or} = \sigma_{i\to d} = 0$. All G2V PEVs charge until they reach $SOE = 1$. Then they are transferred to the Idle category. Similarly, V2G PEVs discharge until $SOE = 0.5$. Then they are transferred to the Idle category. Figure 3 shows that PEVs tend to accumulate in the Idle category at the boundary points $SOE = 0.5$ and $SOE = 1$.

TABLE II. State Space symbols

Symbol	Description
k	Discrete time index
$X(k)$	State: number of PEVs in bins
$U(k)$	Control input (flow Idle-G2V and Idle-V2G)
$Y(k)$	Output vector (eg: total power)
$S(k)$	Uncontrollable input (flow from drivers and $SOE < \underline{SOE}$)

C. Dynamic System Properties

In this section we verify the conservation of mass (i.e. the conservation of PEVs in the system) when there is no external flow, $\sigma_{i\to Or} = 0$.

Proposition 1: The system defined by the coupled dynamics (7), (8), (9) and the boundary conditions in Section II-B verifies the following property when $\sigma_{i\to Or} = 0$:

$$\frac{\partial \mathrm{Nb}_{\mathrm{PEVs}}(t)}{\partial t} = 0$$
$$\text{where } \mathrm{Nb}_{\mathrm{PEVs}}(t) = \int_0^1 [u(x,t) + v(x,t) + w(x,t)]dx$$

Proof 1: When $\sigma_{i\to Or} = 0$, summing Eq (7), (8) and (9) leads to:

$$\frac{\partial}{\partial t}(u+v+w)(x,t) = \frac{\partial}{\partial x}(-q_c u + q_d w)(x,t) \quad (10)$$

By integrating each term of on $x \in [0,1]$, we obtain:

$$\frac{d}{dt}\mathrm{Nb}_{\mathrm{PEVs}}(t) = \Big[(-q_c u + q_d w)(x,t)\Big]_{x=0}^{1}$$
$$= 0 \quad (11)$$

where Eq. (11) comes from the boundary conditions defined in Section II-B. □

III. State Space representation

In this section, we discretize the previous system of PDEs to represent the dynamics in state space form, and we formulate a model predictive controller to track a power signal.

We assume that the aggregator is free to control vehicles in a specific SOE range $[\underline{SOE}, \overline{SOE}] \subset [0,1]$ as shown in Fig. 4. In practice, drivers agree to receive their PEV with any $SOE \in [\underline{SOE}, \overline{SOE}]$ upon departure (i.e. $\underline{\mathrm{SOE}}$ is the minimum SOE when PEVs depart). In exchange, the aggregator manages the charging and discharging of PEVs between these bounds and bids this aggregated storage capacity for load following applications. Figure 4 shows the boundaries of the system: the grey part is not modeled in this framework, and any contribution from this part is considered as an uncontrollable input.

A. State Space model

We divide the space $[\underline{SOE}, \overline{SOE}]$ into N_b bins and discretize the system in time and SOE as shown in Fig. 3. The variables u_j^k, v_j^k and w_j^k denote the number of charging, idle and discharging PEVs in bin j at time k, respectively. The flows between bins are due to transportation dynamics (charging and discharging), controllable flows ($\sigma_{i\to c}$ and $\sigma_{i\to d}$), and uncontrollable flows due to driving ($\sigma_{i\to or}$). We discretize

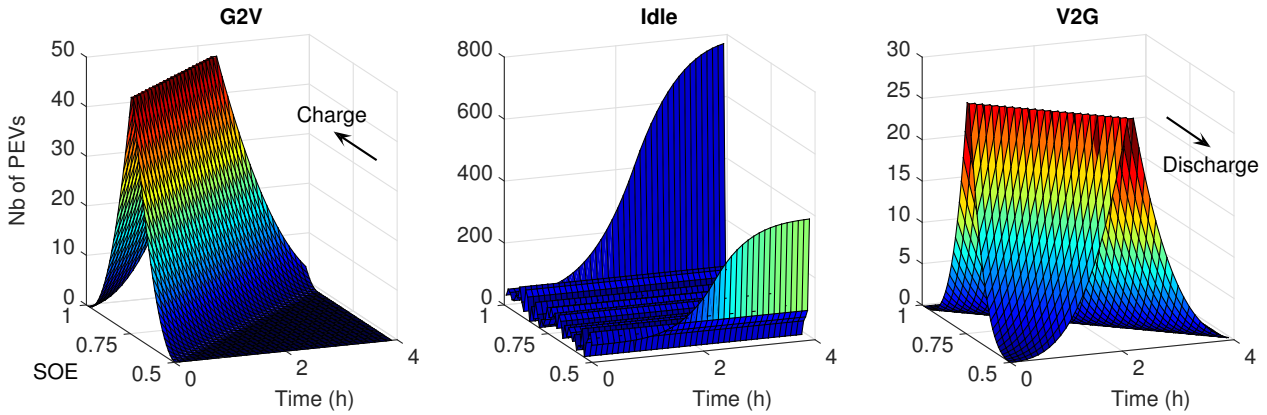

Fig. 3. Evolution of the uncontrolled system of transport PDEs for SOE $\in [0.5, 1]$. All G2V PEVs charge (transported towards high SOE values), and V2G PEVs discharge (transported towards low SOE values).

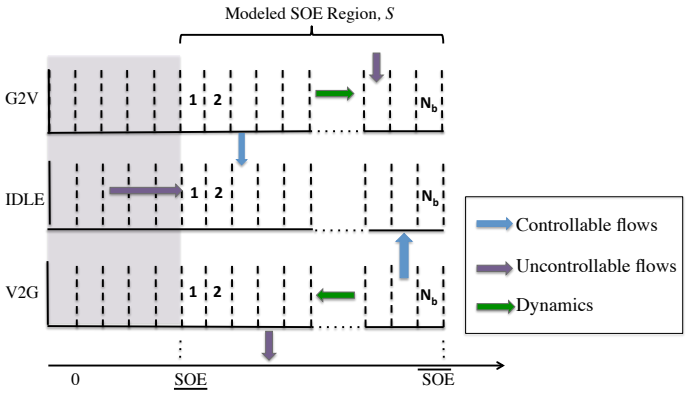

Fig. 4. State transition model

the system with the Lax-Wendroff discretization scheme [24]. The Lax-Wendroff method is a second order explicit discretization scheme. The result for the scalar advection equation $\frac{\partial u}{\partial t} + a\frac{\partial u}{\partial x} = 0$ reads:

$$u_j^{k+1} = u_j^k - \frac{a\Delta t}{2\Delta x}(u_{j+1}^k - u_{j-1}^k) + \frac{a^2\Delta t^2}{2\Delta x^2}(u_{j+1}^k - 2u_j^k + u_{j-1}^k)$$

where Δx is the SOE discretization step, Δt is the time discretization step and $u_j^k = u(j\Delta x, k\Delta t)$.

Reference [23] shows that the Lax-Wendroff scheme is both consistent and conditionally stable for advection PDEs, and reference [16] shows that it performs well for the system of PDEs (7), (8), (9) (error less than 3% in average).

We will use this discretization method in the remainder of this article. Because the numerical scheme is explicit in time, we are able to represent the discretized dynamics of the system with the following state-space model:

$$X(k+1) = \mathbf{A}X(k) + \mathbf{B_u}U(k) + \mathbf{B_s}S(k) \quad (12)$$

$$Y(k) = \mathbf{C}X(k) \quad (13)$$

The variable X represents the state of the system, which is the number of PEVs in each category: ($G2V$, idle, and $V2G$). The variable U is the control input, which controls the flows of PEVs between the three categories. Finally, the variable S is the uncontrollable input, which comes from arrivals and departures of PEVs. This relates to the PDE model described in Section II as follows:

$$X(k) = \begin{bmatrix} u(\cdot, k\Delta t) \\ v(\cdot, k\Delta t) \\ w(\cdot, k\Delta t) \end{bmatrix}, U(k) = \begin{bmatrix} \sigma_{i\to c}(\cdot, k\Delta t) \\ \sigma_{i\to d}(\cdot, k\Delta t) \end{bmatrix}, S(k) = \sigma_{i\to or}(\cdot, k\Delta t)$$

Matrix $\mathbf{A}$ is the dynamic transition matrix, which includes boundary conditions and results from the Lax Wendroff discretization scheme. The output $Y(k) = \mathbf{C}X(k)$ gives the power consumed or supplied by the fleet of PEVs. We assume a uniform power rate p such that:

$$\mathbf{C} = \begin{bmatrix} -p \cdots -p & 0 \cdots 0 & p \cdots p \end{bmatrix} \quad (14)$$

In practice, U gives the SOE distribution of PEVs that are shifted from one charging category to another. In the proposed aggregate model, all the PEVs with the same SOE x at time k are indistinguishable. Thus, to implement the optimal control signal on the real system at time k, the controller chooses $\lfloor \max(0, \sigma_{i\to c}(x, k\Delta t)) \rfloor$ PEVs at random in the idle category and shifts them to the charging category. Similarly, it selects $\lfloor \max(0, -\sigma_{i\to c}(x, k\Delta t)) \rfloor$ PEVs at random in the charging category and shifts them to the idle category. The implementation of $\sigma_{i\to d}$ follows the same control rule. Note that the control signal needs to be rounded before it is implemented.

B. Uncontrollable input and modified State Space model

As specified in Section III, the contribution from drivers and PEVs with $SOE < \underline{SOE}$ is incorporated into the uncontrollable input $\sigma_{i\to Or}(x,t)$ in the PDE model, and $S(k) \in \mathbb{R}^{N_b}$ in the state space model. The uncontrollable flow $S(k)$ only impacts idle cars and can be divided into negative contributions due to arrivals $Arr(k)$, and positive contributions due to departures $Dep(k)$ such that: $S(k) = Arr(k) + Dep(k)$ and a corresponding $\mathbf{B_s} = [0, -I, 0]^T$.

Arrivals into the system comes from drivers who plug-in with $SOE \in [\underline{SOE}, \overline{SOE}]$ and from PEVs reaching $SOE = \underline{SOE}$; this input is completely uncontrollable. In contrary, departures occur at any $SOE \in [\underline{SOE}, \overline{SOE}]$, and depends on the state dynamics and the previous control signals. Consider two distinct control inputs $[U_1(0), ..., U_1(k)]$ and $[U_2(0), ..., U_2(k)]$,

which result respectively in the state values $X_1(k+1)$ and $X_2(k+1)$ at time $k+1$. The distribution of PEVs at time $k+1$ in scenario 1 and scenario 2 are distinct, which implies that $Dep_1(k+1)$ and $Dep_2(k+1)$ may be distinct (i.e. drivers don't get their cars with the same amount of energy). However, the total number of departures, calculated by the sum of departures from each bin as $1^T Dep_1(k+1) = 1^T Dep_2(k+1)$, remains the same in both scenarios We incorporate this characteristic by modeling $Dep \in \mathbb{R}^{N_b}$ by a controllable input with equality constraint $1^T Dep(k) = d(k)$, where $d(k)$ is the expected number of departures at time k. In contrary Arr is modeled as an uncontrollable input. Thus, we augment the state space model as follows:

$$X(k+1) = \mathbf{A}X(k) + \mathbf{B_u}U(k) + \mathbf{B_s}Dep(k) + \mathbf{B_s}Arr(k) \quad (15)$$
$$Y(k) = \mathbf{C}X(k) \quad (16)$$

We will use the state space model (15), (16) in the remainder of this paper.

C. Linear Quadratic Regulator for Signal Tracking

Regulation and load following are ancillary services provided to balance the short term mismatch between generation and demand. Their main difference is their time horizons: while regulation occurs on the second-to-second basis, load following addresses longer-term changes in demand [25], [26]. Regulation and load following are particularly interesting for storage and PEV smart charging because they require fast response and are high price energy markets (see [2], [27]), Since we propose a single discrete charging rate for PEVs that is managed by hysteresis type actions, we choose a longer time horizon and assume that the aggregator provides load following reserves and is located in a unique balancing area.

1) Objective: The problem is formulated as a tracking problem where the reference $P_{des}(t)$ is updated every 15 minutes. The controller penalizes three items: deviation from the reference signal, battery degradation and large controllable flows. Experimental aging studies [28] have shown aging is highly correlated to the integral of power transferred through the battery. Therefore, degradation at time l is measured using $D_g(l) = C_g X(l)$ where C_g is defined as follows:

$$C_g(l) = \begin{bmatrix} p \cdots p & 0 \cdots 0 & p \cdots p \end{bmatrix} \quad (17)$$

The objective function then becomes:

$$J_k(X,U,Y) = \sum_{l=k}^{N+k} \mathbf{Q_{track}}[Y(l) - P_{des}(l)]^2 + U(l)^T \mathbf{R} U(l) + \mathbf{Q_{degrad}}[C_g X(l)]^2 \quad (18)$$

In this formulation R penalizes large control values and thus limits flows between the three states $G2V$, Idle and $V2G$. The relative value of $\mathbf{Q_{track}}$ and $\mathbf{Q_{degrad}}$ shows how much the aggregator prioritizes the compliance to balancing services, versus battery degradation.

2) Linear Quadratic Regulator: The optimal smart charging control comes from the solution of the following LQR - MPC scheme:

$$\min_{U,Dep} J_k = \sum_{l=k}^{N+k} \mathbf{Q_{track}}[Y(l) - P_{des}(l)]^2 + U(l)^T \mathbf{R} U(l) + \mathbf{Q_{degrad}}[C_g X(l)]^2 \quad (19a)$$
$$\text{st } X(l+1) = \mathbf{A}X(l) + \mathbf{B_u}U(l) + \mathbf{B_s}(Dep(l) + Arr(l)) \quad (19b)$$
$$Y(l) = \mathbf{C}X(l) \quad (19c)$$
$$X(l) \geq 0 \quad (19d)$$
$$1^T Dep(l) = d(l),\ Dep(l) \geq 0 \quad (19e)$$
$$X(k) = X_k \quad \text{measured at time k} \quad (19f)$$
$$X(N+k+1) \geq 0 \quad (19g)$$
$$l \in \{k, ..., k+N\}$$

In this MPC formulation, the control horizon is $T_{LQR} = N\Delta t$, the full horizon is $T_f = L\Delta t$ and the MPC is computed for $k \in \{0, ...L-N\}$. At each time step, we consider the control horizon T_{LQR} but implement only the first control action. The MPC stops when we reach the full horizonT_f. We assume P_{des} and d are known or forecasted a priori.

Assumption 1: We assume that the number of departures is always smaller than the number of PEVs in the system, i.e.

$$\sum_{k=0}^{l} [d(k) - 1^T |Arr(k)|] < 1^T [A^l X(0)] \quad \forall l \in \{0, ..., L\}. \quad (20)$$

Proposition 2: Under Assumption 1, the LQR (19) is recursively feasible: for all initially feasible points, X_0, and for all optimal sequences of control inputs, the MPC optimization problem remains feasible at all times.

Proof 2: In practice, this comes directly from the PDE aggregation model, where we formulate boundary and initial conditions to ensure that the problem is well posed (Section II-B). In the case of convection PDEs, this guaranties the conservation of loads. We denote $U_{idle}(l)$ the control sequence that transfers all the PEVs in the Idle category Then, under Assumption 1, we can show that the following control sequence is feasible:

$$U_{idle}(l) = \begin{bmatrix} -I_{N_b} & 0 & 0 \\ 0 & 0 & -I_{N_b} \end{bmatrix} \mathbf{A}X(l) \quad (21)$$

$$Dep(l) = d(l) \frac{\mathbf{A}X(l) + \mathbf{B_u}U(l) + \mathbf{B_s}Arr(l)}{1^T [\mathbf{A}X(l) + \mathbf{B_u}U(l) + \mathbf{B_s}Arr(l)]} \quad (22)$$

The detailed derivation is presented in the Appendix.

IV. Simulations with real-world mobility data

In this section, we demonstrate how the proposed LQR framework applies to a particular case study, and provides general intuition for other cases. We use data presented in reference [29], which comes from more than 2000 non residential charging equipments in Northern California for the year of 2013. Figure 5 shows the maximum capacity of PEVs in the modeled aggregate system (see Fig 4) for a typical weekday.

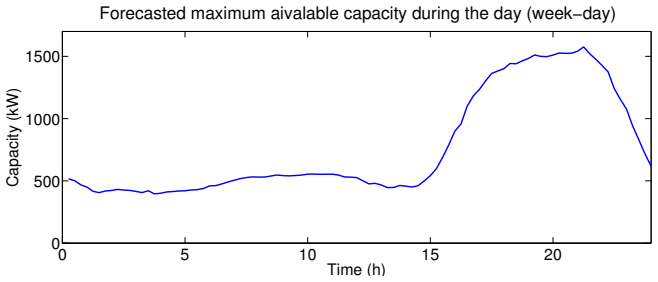

Fig. 5. Maximum power capacity

Thus, we derive the time-dependent forecasted maximum capacity based on the forecasted number of PEVs

$$\overline{Cap} = p \times \mathrm{Nb}_{\mathrm{PEVs}} \tag{23}$$

where p is the power rate of the charging stations and $\mathrm{Nb}_{\mathrm{PEVs}}$ the number of PEVs in the system.

Most Independent System Operators (ISO) have not developed a regulated market for load following yet. Because load following and regulation applications share a lot of similarities (see NERC operating manual [25]), we use existing attributes for regulation markets to base our performance analysis. In particular, if the aggregator bids the available capacity Cap, we assume that the load following signal $P_{des} \in [-Cap, Cap]$ has a zero average over the horizon time. In the following cases studies, we draw a signal uniformly in $[-Cap, Cap]$ and subtract the average to simulate realistic balancing signals.

We measure the performance of the aggregator with the Pennsylvania - New Jersey - Maryland Interconnection (PJM) precision score for regulation services. Specifically, the precision score is defined as follows [30]:

$$\mathrm{Error}(i) = \left| \frac{Y(i) - P_{des}(i)}{P_{des}(i)} \right|, \tag{24}$$

$$\text{Precision score} = 1 - \frac{1}{N} \sum_{i=1}^{N} \mathrm{Error}(i). \tag{25}$$

PJM sets a resource compliance score that includes the precision score defined in (25). In their market eligibility rules, PJM requires that the compliance score be higher than 0.75 [30]. For the purposes of this paper, we use a 0.75 precision score as a metric to represent acceptable performance.

We define the time step Δt = 15min, the time horizon T_f =24h and the control horizon T_{LQR} =4h. Every 15 minutes, the values of P_{des} and d are updated for the next four following hours, a new control sequence is computed based on the LQR (19) for the next four following hours, and only the first control response is executed. This MPC algorithm is iterated until it reaches the time horizon T_f =24h. In the next section, we show how to tune the controller parameters to satisfy the minimum 0.75 precision score condition.

A. Impact of the LQR parameters

In the LQR (19), the parameters $\mathbf{R}$, $\mathbf{Q_{track}}$ and $\mathbf{Q_{degrad}}$ penalize, respectively, large control values, large deviations from the reference signal and large numbers of non-idle cars. These parameters must be tuned to meet the aggregator's objectives. Figure 6 depicts a signal P_{des} between $[-\overline{\mathrm{Cap}}, \overline{\mathrm{Cap}}]$.

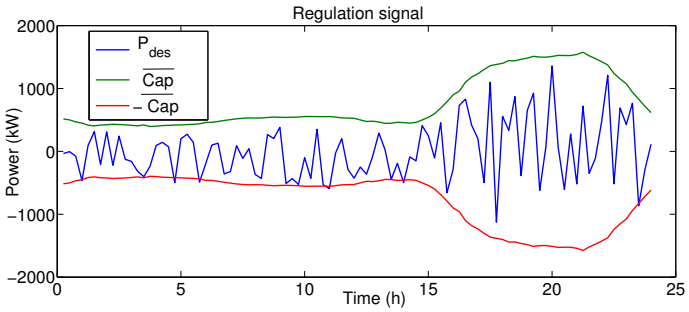

Fig. 6. Load Following signal (every 15min)

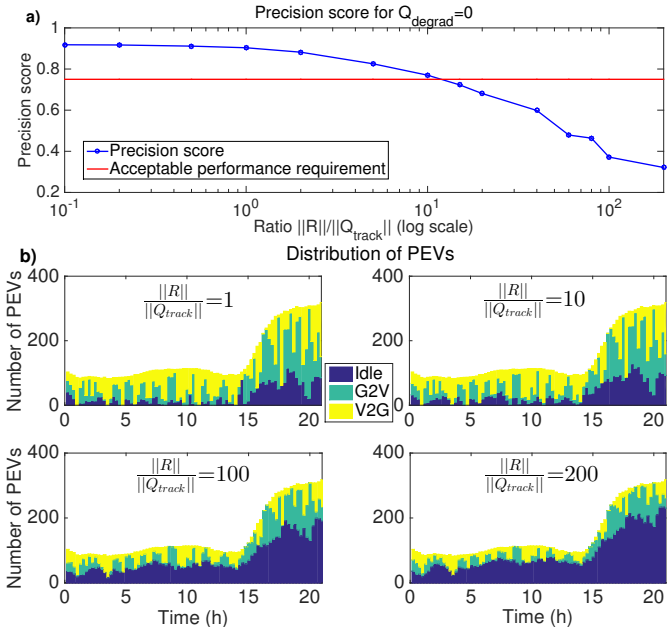

Fig. 7. (a) Precision score and (b) number of PEVs in each charging category for $\mathbf{Q_{degrad}} = 0$ and varying $\frac{||\mathbf{R}||}{||\mathbf{Q_{track}}||}$

The signal is zero-mean over the entire horizon, it is updated every 15 minutes and sent to the aggregator. We assume $\underline{SOE} = 0.8$, $\overline{SOE} = 0.95$. Figure 7a shows the precision score for different ratios $\frac{||\mathbf{R}||}{||\mathbf{Q_{track}}||}$ and $\mathbf{Q_{degrad}} = 0$. As expected, the tracking improves when the ratio $\frac{||\mathbf{R}||}{||\mathbf{Q_{track}}||}$ decreases and in this specific case study, the aggregator meets the acceptable performance requirement for $\frac{||\mathbf{R}||}{||\mathbf{Q_{track}}||} \leq 10$. Figure 7b shows the number of PEVs during the day in each category G2V, V2G or Idle and Table III shows the precision score for four different ratios. The number of idle PEVs tends to increase when less importance is given to tracking, however this has an impact on the aggregator performance and Table III shows that only $\frac{||\mathbf{R}||}{||\mathbf{Q_{track}}||} \leq 10$ satisfies the acceptable performance requirement.

Figure 8a shows the precision score for different ratios of $\frac{||\mathbf{Q_{degrad}}||}{||\mathbf{Q_{track}}||}$ and $R = 0$, Fig 8b visualizes the distribution of PEVs.

TABLE III. Precision scores

$\|\|R\|\|/\|\|\mathbf{Q_{track}}\|\|$	1	10	100	200
Precision Score	0.91	0.77	0.40	0.26

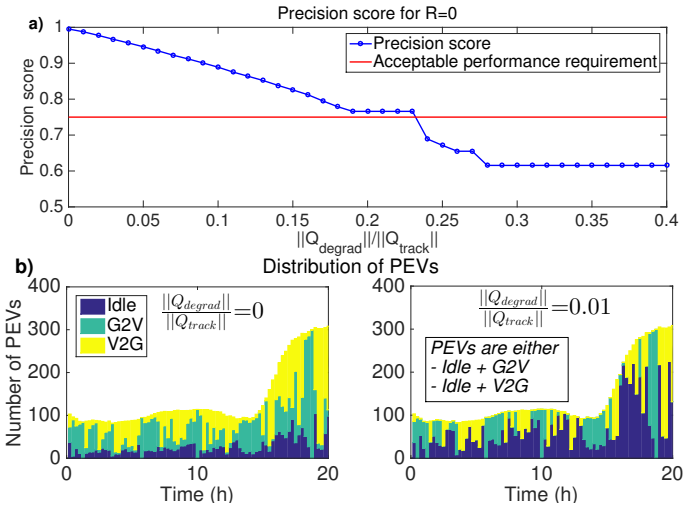

Fig. 8. (a) Precision score and (b) number of PEVs in each charging category for $R = 0$ and varying $\frac{||\mathbf{Q_{degrad}}||}{||\mathbf{Q_{track}}||}$

As before, the tracking improves when the ratio $\frac{||\mathbf{Q_{degrad}}||}{||\mathbf{Q_{track}}||}$ decreases. The effect of $||\mathbf{Q_{degrad}}|| > 0$ is to limit the number of PEVs in the G2V and V2G categories. Figure 8b shows that when $||\mathbf{Q_{degrad}}|| > 0$, one of the G2V or V2G categories is empty at each time step: a positive reference signal is attained with only V2G PEVs and a negative reference signal is attained with only G2V categories, which is the minimum-degradation solution to attain this signal.

B. Impact of the SOE range $[\underline{SOE}, \overline{SOE}]$

As stated in Section III, $[\underline{SOE}, \overline{SOE}]$ defines the boundaries of the system. The lower bound $\underline{SOE}$ comes from a tradeoff between flexibility in driver mobility and flexibility in storage capacity for the aggregator. Figure 9 shows the performance of the aggregator for different values of $\underline{SOE}$, when $\overline{SOE} = 0.95$ is fixed. The green curve illustrates a pessimistic case, where the reference signal is always positive $P_{des} = 0.7\overline{\text{Cap}}$ (i.e. not zero mean) and shows that the aggregator is not able to meet the requirements for $\underline{SOE} \geq 0.5$. The aggregator looses flexibility as the interval $[\underline{SOE}, \overline{SOE}]$ becomes narrower. Let T_{V2G}^{max} denote the longest time period a PEV can stay in the V2G category, i.e. can produce a positive balancing signal. According to Equations (1) and (2), for a constant power p:

$$T_{V2G}^{max}(\underline{SOE}) = [\overline{SOE} - \underline{SOE}]\frac{\eta E_{max}}{p}. \tag{26}$$

Thus, for high values of SOE, the aggregator is unable to track an all positive reference signal, which results in low precision scores when $P_{des} = 0.7\overline{\text{Cap}}$.

The blue curve shows the average and the interquartile range (IQR) error bars of the precision score after 50 simulations of zero-mean reference signals. In this case, simulated reference signals fluctuate between positive and negative values, and a small *SOE* range suffices to create short charge and discharge cycles to track the load following signal. However, IQR error bars show that the statistical dispersion increases as the *SOE* range narrows, and the risk to violate the acceptable performance requirement increases. In particular, the aggregator is unable to meet the acceptable performance requirement in more than 25% of cases when $\underline{SOE} \geq 0.85$.

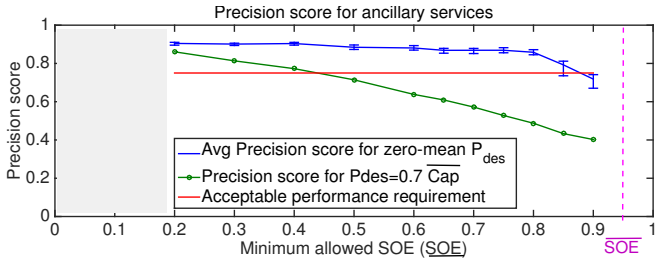

Fig. 9. Average precision score and IQR error bars for different values of $\underline{SOE}$

C. Analysis on capacity bidding

In this section we are interested in finding the best capacity to bid C_{bid}. We assume the aggregator bids a percentage α of its available capacity $\overline{\text{Cap}}$:

$$C_{bid}(\alpha) = \alpha\overline{\text{Cap}} \tag{27}$$

We seek to examine the impact of conservative bidding strategies $\alpha < 1$ versus aggressive bidding strategies $\alpha > 1$.

Figure 10 shows simulation results for $\alpha \in [0, 1.5]$, $\underline{SOE} = 0.75$, $||\mathbf{Q_{track}}|| = ||R||$, and $\mathbf{Q_{degrad}} = 0$. For each α, we simulate 400 reference signals $P_{des} \in [-C_{bid}(\alpha), C_{bid}(\alpha)]$, and we compute the average precision score and the interquartile range. We compare this result with the precision score obtained for the worst-case scenario where $P_{des} = C_{bid}(\alpha) = \alpha\overline{Cap}$. Figure 10b shows that the reference signal generally does not attain the maximum bid capacity, and the average performance of the aggregator is higher than 75% for $\alpha \in [0, 1.5]$. The statistical dispersion tends to increase when α increases, and the aggregator is able to meet the acceptable performance requirement in more than 75% of cases, only when $\alpha \in [0, 1.2]$. This shows that the aggregator could bid more than its actual capacity, and still reach the necessary precision score with a high probability.

However in the worst case scenario, the aggregator cannot bid more that 50% of its capacity. Figure 10a shows the cumulative power during the day when $P_{des} = C_{bid}(\alpha) = \alpha\overline{\text{Cap}}$. The total supplied power increases when α increases, until it attains a maximum reachable power around 1MW: the aggregator is not able to provide an all-positive or all-negative signal during the day. This example justifies that it is essential that the aggregator participates in a market with zero average signals and it confirms the relevance of balancing markets.

V. Conclusion

In this article we propose a novel state space modeling framework for large fleets of PEVs with discrete charging rate. First we aggregate PEVs in three different states, namely G2V, idle and V2G. We derive the dynamics of the fleet as a system of three coupled PDEs, with uncontrollable flows coming from drivers. We use a Lax Wendroff discretization to transform the system of PDEs into a state space representation, where the flows between the three different charging categories are controlled. We propose a Linear Quadratic Regulator

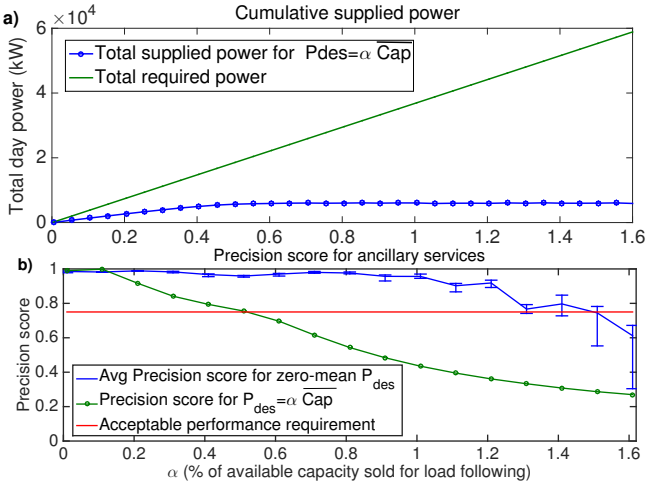

Fig. 10. Average precision score and IQR error bars for different values of α

with the objective to track a power signal, while respecting drivers' mobility constraints. We use Model Predictive Control techniques to solve this problem in real time. We perform various case studies and examine how the performance of the aggregator depends on LQR parameters, drivers' flexibility and capacity bidding strategies. These examples show that the system is particularly adapted to load following, with zero-mean reference signals.

APPENDIX

Proof of Proposition 2:

We assume that $X(0) \geq 0$ and that Assumption 1 is verified. Then, we show that the problem is feasible with the control sequence described in Section III-C2. We consider $k \in \{0,...,N\}$, and apply the control sequence $U_{idle}(k)$ at time k:

$$\begin{aligned} &X(k+1) \\ &= \mathbf{A}X(k) + \mathbf{B_u}U_{idle}(k) + \mathbf{B_s}(Dep(k) + Arr(k)) \\ &= \begin{bmatrix} \mathbf{A}_{V2G}u(k) \\ \mathbf{A}_{idle}v(k) \\ \mathbf{A}_{G2V}w(k) \end{bmatrix} + \begin{bmatrix} -\mathbf{A}_{V2G}u(k) \\ \mathbf{A}_{V2G}u(k) + \mathbf{A}_{G2V}w(k) \\ -\mathbf{A}_{G2V}w(k) \end{bmatrix} - \begin{bmatrix} 0 \\ Dep(k) + Arr(k) \\ 0 \end{bmatrix} \\ &= \begin{bmatrix} 0 \\ \mathbf{A}_{V2G}u(k) + \mathbf{A}_{G2V}w(k) + \mathbf{A}_{idle}v(k) - Dep(k) - Arr(k) \\ 0 \end{bmatrix} \end{aligned}$$

$$\begin{aligned} 1^T X(k+1) = \quad & 1^T[\mathbf{A}_{V2G}u(k) + \mathbf{A}_{G2V}w(k) + \mathbf{A}_{idle}v(k)] \\ & -1^T(Dep(k) + Arr(k)) \\ = \quad & 1^T X(k) - d(k) + 1^T|Arr(k)| \end{aligned} \tag{28}$$

The last equality results from the system dynamics properties: the matrices $\mathbf{A}_{V2G}$,$\mathbf{A}_{Idle}$ and A_{G2V} are obtained from the discretization of convection PDEs, which ensure the conservation of loads. Then:

$$1^T X(k+1) - 1^T X(k) = 1^T|Arr(k)| - D(k)$$

Then, by induction:

$$1^T X(k+1) - 1^T X(0) = \sum_{l=0}^{k} 1^T|Arr(l)| - D(l) \tag{29}$$

Assumption 1 and relations (28), (29) give:

$$\begin{aligned} 1^T X(k+1) &> 0 \\ 1^T X(k) - d(k) + 1^T|Arr(k)| &> 0 \end{aligned} \tag{30}$$

We define:

$$\begin{aligned} Dep(k) &= d(k)\frac{\mathbf{A}_{V2G}u(k) + \mathbf{A}_{G2V}w(k) + \mathbf{A}_{idle}v(k) + |Arr(k)|}{1^T[A_{V2G}u(k) + \mathbf{A}_{G2V}w(k) + \mathbf{A}_{idle}v(k) + |Arr(k)|} \\ &= d(k)\frac{\mathbf{A}_{V2G}u(k) + \mathbf{A}_{G2V}w(k) + \mathbf{A}_{idle}v(k) + |Arr(k)|}{1^T[X(k) + |Arr(k)|]} \end{aligned}$$

We conclude:

$$1^T Dep(k) = d(k) \tag{31}$$

$$Dep(k) \geq 0 \tag{32}$$

$$\begin{aligned} X(k+1) &= \begin{bmatrix} 0 \\ \mathbf{A}_{V2G}u(k) + \mathbf{A}_{G2V}w(k) + \mathbf{A}_{Idle}v(k) + |Arr(k)| \times \mathfrak{G} \\ 0 \end{bmatrix} \\ &\geq 0 \end{aligned} \tag{33}$$

where

$$\mathfrak{G} = 1 - \frac{d(k)}{1^T[X(k) + 1^T|Arr(k)|]} \tag{34}$$

where the last inequality comes from relation (30).
Equations (31), (32), (33) show that the problem is feasible at time k. □

ACKNOWLEDGMENT

We would like to thank Chargepoint LLC. for providing the data used in this study.

REFERENCES

[1] D. B. Richardson, "Electric vehicles and the electric grid:a review of modeling approaches, impacts, and renewable energy integration," *Renewable & Sustainable Energy Reviews*, vol. 19, pp. 247–254, 2013.
[2] W. Kempton and J. Tomić, "Vehicle-to-grid power fundamentals: Calculating capacity and net revenue," *Journal of power sources*, vol. 144, no. 1, pp. 268–279, 2005.
[3] A. Langton and N. Crisostomo, "Vehicle-grid integration: A vision for zero-emission transportation interconnected throughout california's electricity system," California Public Utilities Commission, Tech. Rep. R. 13-11-XXX, 2013.
[4] D. Callaway and I. Hiskens, "Achieving controllability of electric loads," *Proceedings of the IEEE*, vol. 99, no. 1, pp. 184–199, Jan. 2011.
[5] K. Clement, E. Haesen, and J. Driesen, "Coordinated charging of multiple plug-in hybrid electric vehicles in residential distribution grids," in *Power Systems Conference and Exposition, 2009. PSCE '09. IEEE/PES*, March 2009, pp. 1–7.
[6] E. Sortomme, M. Hindi, S. MacPherson, and S. Venkata, "Coordinated charging of plug-in hybrid electric vehicles to minimize distribution system losses," *IEEE Transactions on Smart Grid*, vol. 2, no. 1, pp. 198–205, March 2011.
[7] J. Rivera, P. Wolfrum, S. Hirche, C. Goebel, and H.-A. Jacobsen, "Alternating direction method of multipliers for decentralized electric vehicle charging control," in *2013 IEEE 52nd Annual Conference on Decision and Control (CDC)*, Dec 2013, pp. 6960–6965.
[8] L. Gan, U. Topcu, and S. H. Low, "Optimal decentralized protocol for electric vehicle charging," *IEEE Transactions on Power Systems*, vol. 28, no. 2, pp. 940–951, 2013.
[9] Z. Ma, D. S. Callaway, and I. A. Hiskens, "Decentralized charging control of large populations of plug-in electric vehicles," *IEEE Transactions on Control Systems Technology*, vol. 21, no. 1, pp. 67–78, 2013.

[10] C. L. Floch, F. Belletti, S. Saxena, A. Bayen, and S. Moura, "Distributed optimal charging of electric vehicles for demand response and load shaping," in *2015 IEEE 54th Annual Conference on Decision and Control (CDC)*, 2015.

[11] *Standard J1772-201210*, SAE International, 2012.

[12] A. Y. Saber and G. K. Venayagamoorthy, "Intelligent unit commitment with vehicle-to-grid—a cost-emission optimization," *Journal of Power Sources*, vol. 195, no. 3, pp. 898–911, 2010.

[13] L. Gan, U. Topcu, and S. H. Low, "Stochastic distributed protocol for electric vehicle charging with discrete charging rate," in *Power and Energy Society General Meeting, 2012 IEEE*. IEEE, 2012, pp. 1–8.

[14] N. Rotering and M. Ilic, "Optimal charge control of plug-in hybrid electric vehicles in deregulated electricity markets," *IEEE Transactions on Power Systems*, vol. 26, no. 3, pp. 1021–1029, Aug 2011.

[15] S. Bashash and H. Fathy, "Transport-based load modeling and sliding mode control of plug-in electric vehicles for robust renewable power tracking," *IEEE Transactions on Smart Grid*, vol. 3, no. 1, pp. 526–534, March 2012.

[16] C. Le Floch, F. Di Meglio, and S. Moura, "Optimal charging of vehicle-to-grid fleets via pde aggregation techniques," *American Control Conference*, 2015.

[17] S. Bashash and H. Fathy, "Modeling and control insights into demand-side energy management through setpoint control of thermostatic loads," in *American Control Conference (ACC), 2011*, June 2011, pp. 4546–4553.

[18] J. L. Mathieu, S. Koch, and D. S. Callaway, "State estimation and control of electric loads to manage real-time energy imbalance," *IEEE Transactions on Power Systems*, vol. 28, no. 1, pp. 430–440, 2013.

[19] S. Moura, J. Bendtsen, and V. Ruiz, "Parameter identification of aggregated thermostatically controlled loads for smart grids using pde techniques," *International Journal of Control*, vol. 87, no. 7, pp. 1373–1386, 2014.

[20] S. Bansal, M. N. Zeilinger, and C. J. Tomlin, "Plug-and-play model predictive control for electric vehicle charging and voltage control in smart grids," in *2014 IEEE 53rd Annual Conference on Decision and Control (CDC)*. IEEE, 2014, pp. 5894–5900.

[21] C.-T. Li, C. Ahn, H. Peng, and J. Sun, "Synergistic control of plug-in vehicle charging and wind power scheduling," *IEEE Transactions on Power Systems*, vol. 28, no. 2, pp. 1113–1121, May 2013.

[22] A. D. Giorgio, F. Liberati, and S. Canale, "Electric vehicles charging control in a smart grid: A model predictive control approach," *Control Engineering Practice*, vol. 22, pp. 147 – 162, 2014. [Online]. Available: http://www.sciencedirect.com/science/article/pii/S0967066113001871

[23] J. C. Strikwerda, *Finite difference schemes and partial differential equations*. Siam, 2004.

[24] R. J. LeVeque, *Finite volume methods for hyperbolic problems*. Cambridge university press, 2002, vol. 31.

[25] NERC operating manual. [Online]. Available: http://www.nerc.com

[26] E. Ela, M. Milligan, and B. Kirby, "Operating reserves and variable generation," *Contract*, vol. 303, pp. 275–3000, 2011.

[27] W. Kempton and J. Tomić, "Vehicle-to-grid power implementation: From stabilizing the grid to supporting large-scale renewable energy," *Journal of Power Sources*, vol. 144, no. 1, pp. 280–294, 2005.

[28] S. B. Peterson, J. Apt, and J. Whitacre, "Lithium-ion battery cell degradation resulting from realistic vehicle and vehicle-to-grid utilization," *Journal of Power Sources*, vol. 195, no. 8, pp. 2385–2392, 2010.

[29] E. C. Kara, J. S. Macdonald, D. Black, M. Bérges, G. Hug, and S. Kiliccote, "Estimating the benefits of electric vehicle smart charging at non-residential locations: A data-driven approach," *Applied Energy*, vol. 155, pp. 515 – 525, 2015.

[30] PJM, "Manual 12: Balancing operations," 2014. [Online]. Available: http://www.pjm.com/ /media/documents/manuals/m12.ashx